Applied Catalysis B: Environmental 205 (2017) 302–309

Contents lists available at ScienceDirect

Applied Catalysis B: Environmental

journal homepage: www.elsevier.com/locate/apcatb

Impact of pH on the kinetics of photocatalytic oxidation of 2,4-dichlorophenoxy acetic acid in a fluidized bed photocatalytic reactor

Reza Rezaei, Madjid Mohseni*

Department of Chemical and Biological Engineering, University of British Columbia, 2360 East Mall, Vancouver, BC, V6T 1Z3 Canada

ARTICLE INFO

Article history:
Received 24 August 2016
Received in revised form 9 December 2016
Accepted 12 December 2016
Available online 15 December 2016

Keywords:
Photocatalytic oxidation
pH
Kinetic
Hydroxyl radicals
Positive holes

ABSTRACT

The impact of pH on the kinetics of photocatalytic oxidation of 2,4-dichlorophenoxy acetic acid (2,4-D) was investigated. Experiments were performed in fluidized bed photocatalytic reactor using TiO_2 photocatalyst spheres. The rate of oxidation was affected by the solution pH. In acidic medium, according to the kinetic model, the rate of oxidation was higher because the rate constant was directly related to UV intensity (I); whereas this relationship reduced to a functional square root (i.e., $I^{1/2}$) at pH 7. In addition, pH resulted in changing the photocatalytic oxidation mechanism. At pH 7, the photocatalytic oxidation took place away from the photocatalyst surface, the oxidation rate followed first order kinetics. Under acidic condition, on the other hand, the oxidation mostly took place on the surface of photocatalyst and the rate of oxidation followed a combination of the Langmuir-Hinshelwood and first order kinetic models.
© 2016 Elsevier B.V. All rights reserved.

1. Background

Photocatalysis is a process where a semiconductor is activated by UV radiation to produce hydroxyl radicals. Hydroxyl radicals are bound or diffuse into the solution to act as the primary oxidants in the photocatalytic system. Hoffmann et al. [1] analyzed the kinetics of photocatalytic oxidation of several acidic and non-acidic organic compounds. Assuming that all reactions take place on the surface of photocatalyst, the authors used the Langmuir-Hinshelwood (L-H) kinetic model to express the photocatalytic oxidation rates. While there was a verification for the presence of hydroxyl radical in the solution (OH°_{aq}) [1–5], Hoffmann et al. [1] did not consider OH°_{aq} oxidation in their kinetics analysis.

There is strong evidence for the contribution of OH°_{aq} in photocatalytic oxidation [1,6,7], even though OH°_{aq} has been considered equal to adsorbed hydroxyl radical (OH°_{ads}) in many kinetic studies. This is probably due to the difficulty in assessing the role of OH°_{aq} given the very short life of hydroxyl radicals and their high activity, resulting in OH°_{aq} diffusing a very short distance from the surface of the photocatalyst before being consumed [4,8–10].

Tunesi et al. [11] studied the photocatalytic oxidation pathways and showed that there is a marked difference between decomposition via charge transfer on the surface of photocatalyst, and oxidation via OH°_{aq} attack in the solution. The different photocatalytic oxidation pathways can be explained on the basis of the solution pH. Tunesi et al. [11] made a connection between pH effect on TiO_2 adsorption capability and photocatalytic mechanism, but the authors could not delineate how the kinetic of the photocatalytic oxidation changes according to the solution pH.

While several studies have been performed around the effect of pH on photocatalytic oxidation [11–13], detailed information on the effect of pH on photocatalytic oxidation kinetics is still lacking. The effect of pH on photocatalytic mechanism needs more thorough analysis in order to gain an understanding of the impact of pH. The aim of this research has been to develop and experimentally validate a kinetic model to interpret the photocatalytic oxidation at different pH. We analyze and demonstrate that the photocatalytic oxidation kinetic models change according to the solution pH. Furthermore, we illustrate how pH impacts various kinetic parameters. 2,4-D was selected as a model micropollutant due to its specific characteristics; its propensity for adsorption on the surface of photocatalytic spheres and generating intermediates with low affinity for adsorption [14].

2. Theory of the pH effect on photocatalytic mechanism

Photocatalytic removal of contaminants includes two main processes; adsorption and photocatalytic oxidation [7,15,16]. The

* Corresponding author.
E-mail address: madjid.mohseni@ubc.ca (M. Mohseni).

http://dx.doi.org/10.1016/j.apcatb.2016.12.038
0926-3373/© 2016 Elsevier B.V. All rights reserved.

Nomenclature

Arabic

a_c	Illuminated photocatalytic spheres area, m^2.
a_s	Photocatalytic spheres surface area, m^2.
I	UV intensity, einstein. m^{-2} min^{-1}
k	Reaction rate constant
K	Equilibrium adsorption constant, m^3g^{-1}
pK_a	Acid dissociation constant

Greek

β	Kinetic parameter
κ	Kinetic parameter, m^3g^{-1}

Subscripts (Arabic numbers refer to the reactions number)

ex	Refers to electron hole pair generation
rec	Refers to electron hole pair recombination
aq	Indicates that the parameter or species is non-adsorbed
ads	Indicates that the parameter or species is adsorbed on the surface of photocatalyst

photocatalytic oxidation mechanism may be described by the following sequence of elementary reaction steps: excitation, recombination, charge trapping, generation of oxidant species, and organic decomposition. Below are brief analyses of each of the two processes of adsorption and oxidation:

2.1. Adsorption

Adsorption encompasses the adsorption of reactant and water (Eqs. (1) and (2)). In an aqueous medium, the surface of TiO_2 is readily hydroxylated. Ti cations can bond to oxygen atoms of water molecules which are adsorbed on the surface of the photocatalyst and dissociated to OH^- groups (Eq (2)).

$$Site + R_L \rightleftharpoons R_{ads} \quad \left(K = k_1/k_{-1}\right) \tag{1}$$

$$TiO_2 + H_2O \rightleftharpoons Ti - OH^- + H_s^+ \quad (k_2) \tag{2}$$

where R_L and R_{ads} are non-adsorbed and adsorbed reactants, respectively. Attributable to TiO_2 amphoteric behaviour, pH plays the main role in the adsorption of reactants [13]. The effect of pH on adsorption can be explained on the basis of the TiO_2 zero-point charge (zpc). The TiO_2 surface is positively charged ($TiOH_2^+$) at pH< pH_{zpc}, whereas it is negatively charged (TiO^-) at pH>pH_{zpc}; hence, influencing the micropollutant adsorption and its degradation pathways [11,17].

$$pH < pH_{zpc} \quad \mathrm{Ti - OH} + H^+ \rightleftarrows \mathrm{TiOH_2^+} \quad (k_3) \tag{3}$$

$$pH > pH_{zpc} \quad \mathrm{Ti - OH} + OH^- \rightleftarrows \mathrm{Ti} - O^- + H_2O \quad (k_4) \tag{4}$$

The electrostatic repulsion between the reactant anion and the oxide surface reduces the adsorption and increases the distance between reactant and the photocatalyst surface. The increased distance between the reactant and the photocatalyst causes reduced direct charge transfer.

2.2. Photocatalytic oxidation

Photocatalytic reaction is initiated when UV radiation activates a photocatalyst. UV radiation excites the electrons in the valence band to the conduction band, resulting in the formation of a positive hole (h_{vb}^+) in the valence band and an electron (e_{cb}^-) in the conduction band.

$$TiO_2 \xrightarrow{h\nu} TiO_2\left(e_{cb}^- + h_{vb}^+\right) \quad (k_{ex}) \tag{5}$$

The overall rate of photocatalytic reactions in aqueous systems is governed by the capture of electrons and positive holes, and also by the electron–hole re-combination (e^--h^+), Eqs. (6)–(10) [1,12,18,19]. Charge carrier trapping suppresses re-combination of the electron-hole pair, and increases the lifetime of the separated electron and hole. The electron in the conduction band reduces adsorbed oxygen to produce supper oxide (Eq. (9)), whereas the positive hole oxidizes either the reactant directly (see Eq. (10)), or the adsorbed water to produce hydroxyl radical (•OH), as shown in Eq. (7) [1,20,21].

$$e_{cb}^- + h_{vb}^+ \rightarrow heat \quad (k_{rec}) \tag{6}$$

$$Ti^{4+}OH + h^+ \rightleftharpoons Ti^{4+}OH^\circ \quad (k_7/k_{-7}) \tag{7}$$

$$Ti^{4+} + e^- \rightleftharpoons Ti^{3+} \quad (k_8) \tag{8}$$

$$Ti^{3+} + O_2 \rightleftharpoons Ti^{4+} - O^\circ\ {}^-{}_2 \quad (k_9) \tag{9}$$

$$R_{ads} + h^+ \rightarrow R^\bullet{}_{ads} \quad (k_{10}) \tag{10}$$

Rothenberger et al. [22] indicated that pH affects the rate of charge trapping. It was also shown that the hole trapping occurs on a time scale (nano-second) much longer than that for the electron (pico-second) [22]. Therefore, we can assume low recombination rate and high oxidation rate via positive holes on TiO_2 at low pH. As will be shown later, this conclusion of the effect of pH on the trapping charge process plays the major role in the kinetic analysis.

pH also impacts the generation of $OH^\circ{}_{aq}$; at pH > pH_{zpc} hydroxyl radicals can diffuse into the solution (see Eq. (11)) to produce $OH^\circ{}_{aq}$. In contrast, at acidic pH (pH 3) the diffusion rate is very low [4].

$$Ti^{4+}OH^\bullet \xrightarrow{h\nu} Ti^{4+} + OH^\bullet{}_{aq} \quad (k_{11}) \tag{11}$$

The other oxidant species, which may contribute to the photocatalytic oxidation process, is perhydroxyl radical ($HO^\bullet{}_2$). The reaction for $HO^\bullet{}_2$ formation (see Eq. (12)) is largely pH dependent (the pK_a of perhydroxyl radical is 4.8) [8,12,23]. The contribution of perhydroxyl radical oxidation even at pH 3 has not been considered in this research, because the rate constant of perhydroxyl radical reaction with the reactant is 10^3 times lower than that of the hydroxyl radical oxidation [24].

$$pK_a = 4.8 \quad Ti^{4+} - O^{\bullet -}{}_2 + H^+ \rightleftharpoons \mathrm{Ti}^{4+}(HO^\bullet{}_2) \quad (k_{12}) \tag{12}$$

This review of the effect of pH on the photocatalytic mechanism was used in developing and understanding the kinetics of photocatalytic process in this research. Reactions were selected based on their contribution at different pH.

3. Materials and methods

3.1. Reagents and chemicals

Denatured alcohol (EtOH/MeOH, 85/15%), hydrochloridric acid (36.5%), ammonium hydroxide (30%), glacial acetic acid (HPLC grade, >99.7%), and sodium hydroxide were purchased from Fisher Scientific, Canada. Methanol (HPLC grade, 99.9%), Titanium tetraisopropoxide (TTIP, 97%), 2,4-D (97%), Chitosan ($C_{12}H_{24}N_2O_9$, medium molecular weight, 340 g moL^{-1}) were purchased from Sigma–Aldrich, Canada. Commercial TiO_2 powder Degussa P-25 (88% anatase and 12% rutile, surface area of 54 m^2g^{-1}) was obtained from Evonik-Degussa GmbH, Germany. Reaction mixtures and HPLC mobile phase were prepared with Milli-Q water.

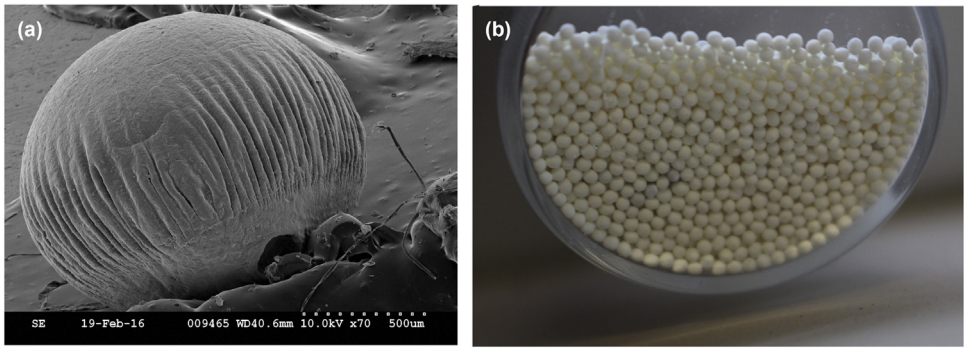

Fig. 1. Photocatalyst spheres, (a) SEM micrograph, (b) after calcination process.

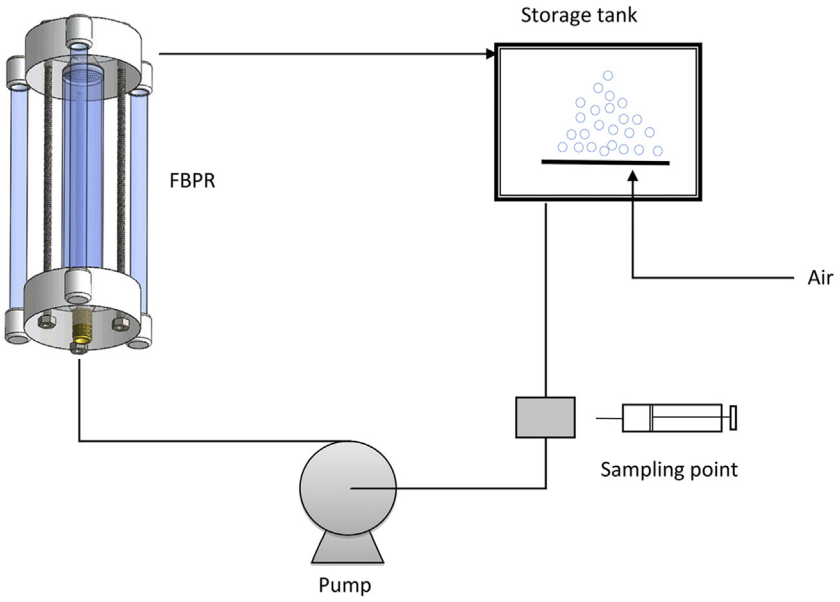

Fig. 2. Fluidized bed photocatalytic reactor set-up.

3.2. Preparation of photocatalyst (template free photocatalyst spheres)

Template free photocatalyst spheres (PSs) were made of sol-gel derived composite TiO_2 as described by Vega et al. [25]. Titanium tetraisopropoxide (TTIP) was used as the precursor. One part of TTIP was slowly added to one part of a solution of denatured ethyl alcohol (81% v/v), water (5% v/v) and HCl (14%v/v). The mixture was magnetically stirred for 2 h. Pre-calcined TiO_2 powder, Degussa P-25, was added to the sol-gel solution and the resulting composite sol-gel (CSG) was vigorously stirred for 16 h to form a homogenous mixture. One part CSG was mixed with two parts polymeric solution made of chitosan and milli-Q water at pH 4.5 to create a suspension needed for sphere formation. The solution was added drop-wise to a basic solution, NH_4OH/water (20:80% v/v), to produce the spheres. The spheres were then dried at 85 °C for 45 h before calcination at 600 °C for 3 h.

3.3. Characterization of photocatalytic spheres

Crystallinity of the photocatalyst spheres was assessed using X-ray diffraction (XRD) analysis (Bruker D8-Advance X-ray, 40 kV and 40 mA). X-ray diffraction patterns were recorded using $CoK\alpha_1$ (λ_1 = 1.5406Å) and $CoK\alpha_2$ (λ_2 = 1.54439Å) over the range 2θ from 5° to 90°, with a scanning speed of 0.016° min^{-1}. Applying the Rietveld refinement method showed that the photocatalyst consists of 71.5% anatase crystalline form.

The specific surface area of the photocatalyst spheres (35.26 $m^2\ g^{-1}$) was determined by the Brunauer–Emmet–Teller (BET) method using nitrogen adsorption/desorption at 77 K and ASAP 2020 software. The Barrett–Joyner–Halender (BJH) method was used to measure the photocatalyst pore volume (0.29 $cm^3\ g^{-1}$) and pore size (24.99 nm).

The microstructural characteristics of the photocatalyst spheres were analysed using a scanning electron microscope (Hitachi S2600 Variable Pressure-SEM). The average diameter of the photocatalyst spheres was 0.90 mm Fig. 1.

3.4. Photocatalytic degradation experiments

Photocatalytic experiments were performed in a fluidized bed photocatalytic reactor (FBPR) set-up, as shown in Fig. 2. The body of the reactor consisted of a quartz tube (150 mm height and 26 mm internal diameter) which was surrounded with three UV lamps (5.7 W at 254 nm, GPH357T5L/4P Light Sources Inc.). The reactor was filled with 25 g PSs and the system was operated at a flow rate of 3.6-3.9 L/min to ensure a maximum bed expansion of about 400% (the optimum value to ensure all the PSs receive the UV radiation). Concentration of dissolved oxygen was maintained constant by sparging air through a storage tank. Two liters of water contaminated with different concentrations of 2,4-D at different pH was

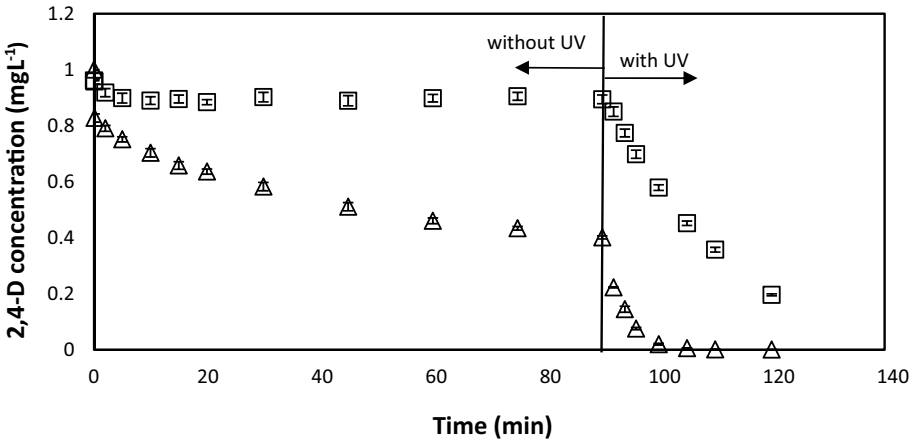

Fig. 3. Photocatalytic oxidation of 2,4-D with the initial concentration of 1 mgL^{-1} in a fluidized bed photocatalytic reactor at (△) pH 3 and (□) pH 7. Error bars represent the standard errors for the triplicate runs.

placed in the storage tank and re-circulated through the reactor, first with the lamps turned off to ensure the adsorption of solutes on the surface of the spheres reached equilibrium. The lamps were turned on after 90 min and samples were taken at different intervals with a total reaction time of 30 min. The samples were taken from the storage tank and filtered through 0.2 μm filter prior to analysis.

3.5. Photocatalytic spheres reactivation

Photocatalytic spheres were reactivated by desorption of organic molecules at high pH. Used 25 g photocatalysts were fluidized by NaOH solution (pH 11) in FBPR. Two liters of NaOH solution was recirculated in the reactor, in the absence of UV radiation and at the same condition used for photocatalytic experimental procedure, for 30 min to desorb 96 ± 2% of organic molecules from the surface of photocatalyst spheres.

3.6. Analytical procedures

The concentration of 2,4-D was quantified using a high-performance liquid chromatograph (HPLC, Dionex 2695) equipped with C-18 column (4-micronmeter particle diameter) and a UV detector. Methanol/water/acetic acid (58%:40%:2%v/v) was used as the mobile phase. The injected sample volume was 100 μL. The flow rate of the mobile phase was 1 mL/min using λ=280 nm UV detection. To determine the charge on TiO_2, the spheres were first ground to form a colloidal suspension (0.002 wt% in water). A Malvern Zetasizer 2000 was used for determining the charge of the photocatalyst.

4. Results and discussions

The zero point charge (Hp_{zpc}) of the photocatalyst spheres has previously been determined to be 6 [26]. This means the photocatalyst surface is positively charged ($TiOH_2^+$) at pH<6, whereas it is negatively charged (TiO^-) at pH>6. 2,4-D, on the other hand, is deprotonated at pH > 2.69 [27] which causes a significant adsorption by the photocatalyst spheres at pH<6 due to electrostatic attraction. At pH>6, however, 2,4-D is repelled by the negative charge of the photocatalyst and there is no adsorption taking place.

Fig. 3 shows the overall removal of 2,4-D at pH 7 and pH 3. The results confirm that the adsorption is not significant at neutral pH, while nearly 60% of the initial 2,4-D is adsorbed on the surface of photocatalyst at pH 3. It is, hence, hypothesized that OH°_{aq} attack is the predominant process for the oxidation of 2,4-D at pH 7, whereas all oxidant species, positive holes (trapped and un-trapped) and free hydroxyl radicals in the solution, contribute towards the degradation of 2,4-D at pH 3. This hypothesis was evaluated through a detailed theoretical analysis and further validated by experimental data.

4.1. Photocatalytic oxidation kinetic analysis at pH 7

Since the adsorption at pH 7 is very negligible, it is assumed that photocatalytic oxidation occurred by the reaction of non-adsorbed reactant and OH°_{aq}, Eq. (13):

$$OH^\bullet_{aq} + R_L \rightarrow R^\bullet_L \quad (k_{aq}) \tag{13}$$

$$r_{pH7} = k_{aq}[R_L][OH^\bullet_{aq}] \tag{14}$$

Therefore, reactions presented earlier through Eqs. (4)–(9), Eqs. (11), and (13) can be considered.

One can denote the trapped positive hole ($[Ti^{IV}OH^\bullet]$) as adsorbed hydroxyl radical OH°_{ads}. Assuming a steady state approximation for the concentration of $OH^\bullet_{aq}$ leads to:

$$\frac{d[OH^\bullet_{aq}]}{dt} = k_{11}[OH^\bullet_{ads}] - k_{aq}[OH^\bullet_{aq}][R_L] - \sum_{i=2}^{n} k_{Ri}[OH^\bullet_{aq}][R_{Li}] \cong 0 \tag{15}$$

$$[OH^\bullet_{aq}] = \frac{k_{11}[OH^\bullet_{ads}]}{k_{aq}[R_L] + \sum_{i=2}^{n} k_{Ri}[R_{Li}]} \tag{16}$$

where R_{Li} and k_{Ri} are 2,4-D intermediates and their rate constants, respectively. To obtain the concentration of $OH^\bullet_{aq}$, it is necessary to have the concentration of $OH^\bullet_{ads}$, which under steady state condition, can be obtained by:

$$\frac{d[OH^\bullet_{ads}]}{dt} = k_7[h^+][TiOH]a_s - k_{-7}[OH^\bullet_{ads}]a_s - k_{11}[OH^\bullet_{ads}]a_s \cong 0 \tag{17}$$

In this analysis, the oxidation of intermediates of 2,4-D on the surface of the catalyst were not considered because the intermediates of 2,4-D oxidation possess pK_a higher than 8 [26]. Because of the high pK_a of intermediates, they are desorbed immediately from the surface of the photocatalyst. This hypothesis was further substantiated by analyzing the concentration of organics desorbed from the surface of photocatalyst during the reactivation process.

One may assume that the photocatalyst hydrolysis by water and adsorption by oxygen reaches an equilibrium before the photocatalytic oxidation starts and will be constant during the process [7]. This means $k_7\,[TiOH] = k_7'$ and $[TiOH] = [TiO^-]$. Therefore:

$$[OH^\bullet_{ads}] = \frac{k_7'[h^+]}{k_{-7} + k_{11}} \tag{18}$$

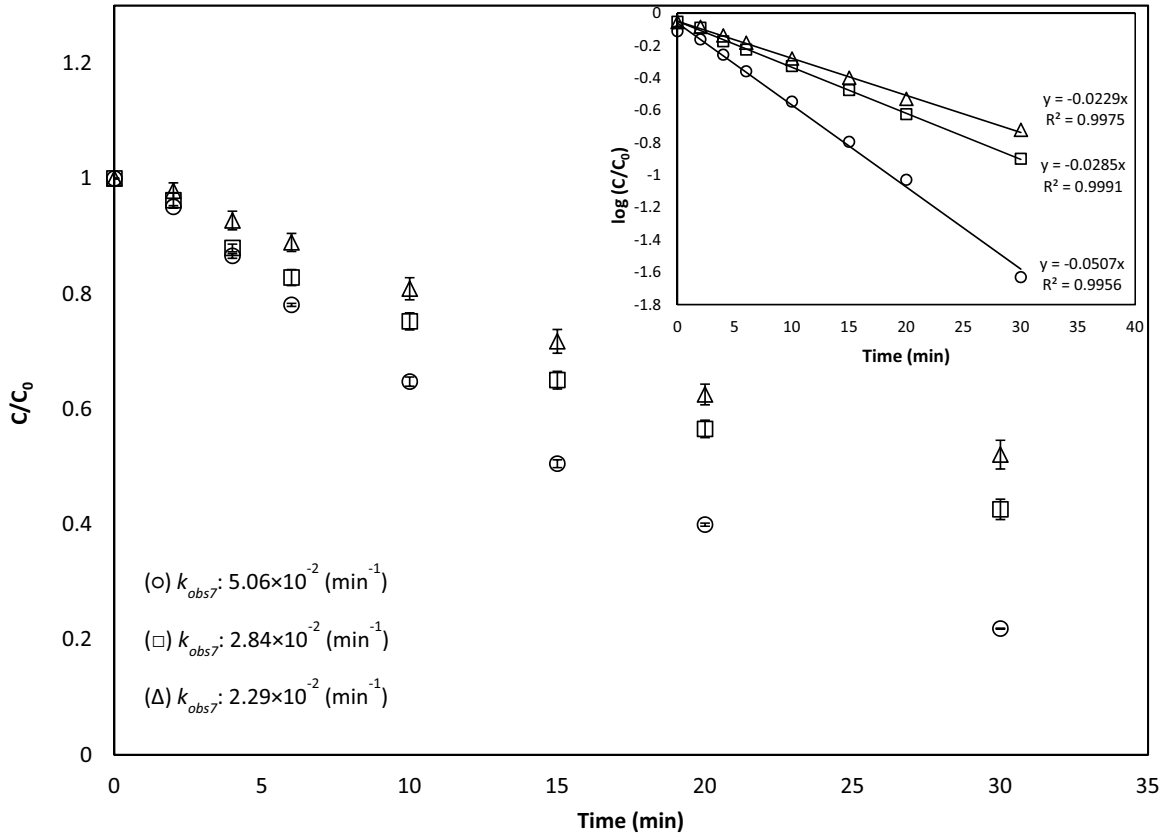

Fig. 4. Photocatalytic oxidation of 2,4-D in a fluidized photocatalytic reactor at pH 7 with different initial concentration of; (○) 1 mgL^{-1}, (□) 4 mgL^{-1}, and (Δ) 7 mgL^{-1}. Error bars represent the standard errors for the triplicate runs. Full lines represent best-fit lines of first order kinetic model.

Similarly, if one uses the steady state approximation for the concentration of h^+, it will lead to:

$$\frac{d[h^+]}{dt} = k_{ex} I a_c - k_{rec}[h^+][e^-]a_s - k_7'[h^+]a_s + k_{-7}[OH^\bullet_{ads}]a_s \cong 0 \quad (19)$$

The formation of Ti^{3+} species, in Eq. (8), is very low in non-acidic solution [3]. In other words, the concentration of e^- is supposed to be high at pH 7. On the other hand, Rothenberger et al. [22] showed that the recombination rate is 10 times faster than h^+ trapping. In conclusion, the concentration of h^+ is high and the recombination rate is fast. Therefore, Eq. (19) can be modified to Eq. (21) based on the following assumption:

$$[h^+] = [e^-] \,\&\, k_{rec}[h^+][e^-]a_s = k_{rec}[h^+]^2 a_s \gg k_7'[h^+]a_s - k_{-7}[OH^\bullet_{ads}]a_s \quad (20)$$

$$\frac{d[h^+]}{dt} = k_{ex} I a_c - k_{rec}\left[h^+\right]^2 a_s \cong 0 \quad (21)$$

Therefore:

$$\left[h^+\right] = \sqrt{\frac{k_x I a_c}{a_s k_{rec}}} \quad (22)$$

$$\left[h^+\right] = \beta\sqrt{I} \text{ and } \beta = \sqrt{\frac{k_{ex} a_c}{a_s k_{rec}}} \quad (23)$$

Hence:

$$[OH^\bullet_{ads}] = \frac{k_7'\beta\sqrt{I}}{k_{-7} + k_{11}} \quad (24)$$

Finally, combining Eqs. (14), (16) and (24), will provide:

$$r_{pH7} = \frac{\beta k_7' k_{11} k_{aq}[R_L]}{\left(k_{aq}[R_L] + \sum_{i=2}^{n} k_{Ri}[R_{Li}]\right)(k_{-7} + k_{11})}\sqrt{I} \quad (25)$$

Hydroxyl radical is a nonselective and very strong oxidant; the rate constants for OH° is generally in the order of 10^9 $M^{-1}s^{-1}$ [7]. Therefore, one can assume that $k_{aq} = k_{Ri}$ simplifying Eq. (25).

$$r_{pH7} = k_{obs7}[R_L] \quad (26)$$

where

$$k_{obs7} = \frac{k_7' k_{11}\left(\frac{k_{ex} a_c}{a_s k_{rec}}\right)^{1/2}}{(k_{-7} + k_{11})[R_{0L}]}\sqrt{I} \quad (27)$$

where R_{0L} is the initial concentration of the reactant, considered equal to the concentration of R_L plus the intermediates present in the system ($[R_L] + \sum_{i=2}^{n}[R_{Li}]$), before CO_2 is formed through complete mineralization.

Eq. (26) shows that the photocatalytic oxidation at pH > pH_{pzc} followed first order kinetic equation with respect to the reactant concentration. It should be noted that k_{obs7} is a function of $\sqrt{I}$ and initial concentration of the reactant (see Eq. (27)).

To validate the kinetic model, an experiment was performed to measure the photocatalytic oxidation rate of 2,4-D at different initial concentrations. Fig. 4 shows that the apparent rate constant (k_{obs7}) decreases by increasing the initial concentration. To correspond the value of the experimental rate constant to the k_{obs7} obtained from the model, there is an inverse relationship between the experimental k_{obs7} and initial concentration, which is in agreement with Eq. (27).

4.2. Photocatalytic oxidation kinetic analysis at pH 3

At pH 3, due to the high adsorption of the reactant, the oxidation mechanism is more complicated. A series of reactions, i.e.,

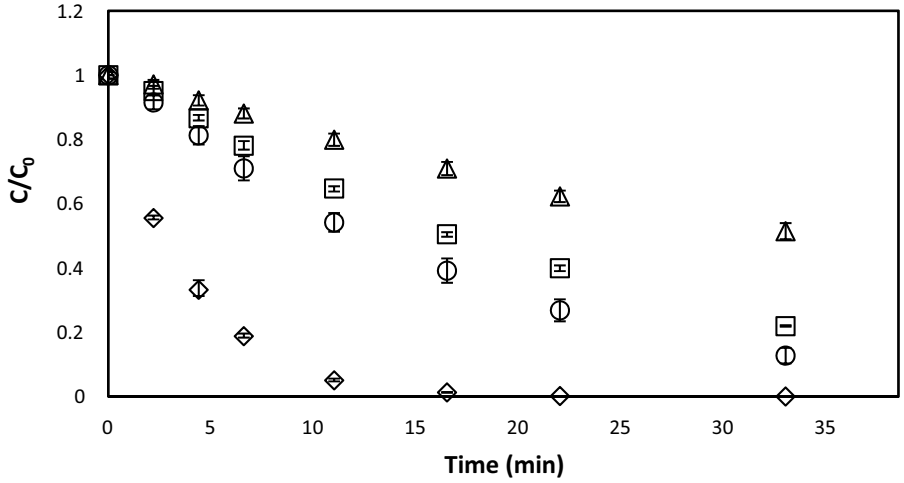

Fig. 5. 2,4-D degradation in a fluidized bed photocatalytic reactor at different pH and initial concentration; (◊) 1 mg L^{-1} 2,4-D at pH 3, (○) 7 mgL^{-1} 2,4-D at pH 3, (□)1 mg L^{-1} 2,4-D at pH 7 and, (Δ) 7 mgL^{-1} 2,4-D at pH 7. Error bars represent the standard errors for the triplicate runs.

Eqs. (1), (3), (5)–(11), and (13), are involved in oxidizing the target contaminant at pH 3. Reactant can be oxidized on the surface of photocatalyst via positive holes (Eqs. (10) and (28)) or in the solution via hydroxyl radical attack (Eq. (13)).

$$Ti^{IV}OH^{\bullet} + R_{ads} \rightarrow Ti^{III} + R^{\bullet}_{ads}\,(k_{ads}) \tag{28}$$

$$R_{ads} + h^{+} \rightarrow R^{\bullet}_{ads}(k_{10}) \tag{10}$$

$$OH^{\bullet}_{aq} + R_L \rightarrow R^{\bullet}_{L}\,(k_{aq}) \tag{13}$$

Therefore, the following three reactions are considered:

$$r_{ads1} = k_{10}\,[R_{ads}]\left[h^{+}\right] a_s \tag{29}$$

$$r_{ads2} = k_{ads}[R_{ads}][OH^{\bullet}_{ads}]a_s \tag{30}$$

$$r_{aq3} = k_{aq}[R_L][OH^{\bullet}_{aq}] \tag{31}$$

where the overall photocatalytic oxidation (r_{pH3}) will be the sum of Eqs. (29) to (31).

Similarly, a steady state approximation for the concentration of h^+ at pH 3 is assumed:

$$\frac{d[h^{+}]}{dt} = k_{ex}Ia_c - k_{rec}[h^{+}][e^{-}]s_p - k_7[TiOH][h^{+}]a_s + k_{-7}[OH^{\bullet}_{ads}]a_s - k_{10}[R_{ads}][h^{+}]a_s \cong 0 \tag{32}$$

The positive hole trapping and recombination rate are dependent on the pH; in the acidic medium, the charge transfer occurs very fast [22]. At pH 3, on the other hand, the high concentration of Ti^{3+} is evidence of a low recombination rate. Therefore, one may assume:

$$k_{rec}[h^{+}]^2 s_p \ll k_7[TiOH][h^{+}]a_s - k_{-7}[OH^{\bullet}_{ads}]a_s + k_{10}[R_{ads}][h^{+}]a_s \tag{33}$$

The concentration of h^+ will then be:

$$[h^{+}] = \frac{k_{ex}Ia_c + k_{-7}[OH^{\bullet}_{ads}]a_s}{k_7[TiOH]a_s + k_{10}[R_{ads}]a_s} \tag{34}$$

Since the consumption rate of e^- is faster than the h^+ trapping rate, the reaction in Eq. (7) is merely on path to generate $OH^{\bullet}_{ads}$. Therefore, one may assume that k_{-7} is very low.

$$\left[h^{+}\right] = \frac{k_{ex}Ia_c}{k_7\,[TiOH]\,a_s + k_{10}\,[R_{ads}]\,a_s} \tag{35}$$

Fujishima et al. [28] studied electron-hole capturing rates and showed that the rate of positive hole capturing by water (k_7) is almost 40 times greater than that with the organic compounds (k_{10}). Moreover, because the number of adsorbed water molecules, due to higher water concentration, is substantially higher than that of 2,4-D ($[TiOH] \gg [R_{ads}]$) one may assume $k_7\,[TiOH] \gg k_{10}\,[R_{ads}]$.

$$r_{ads1} = k_{10}\,[R_{ads}]\left[h^{+}\right] a_s = \frac{k_{10}k_{ex}Ia_c\,[R_{ads}]}{k_7\,[TiOH]} \tag{36}$$

According to Eq. (1), $[R_{ads}]=K\,[R_L][site]$ where $K=k_1/k_{-1}$ and $k_7\,[TiOH] = k'_7$. Therefore,

$$r_{ads1} = k'\,[R_L] \tag{37}$$

where

$$k' = \frac{a_c k_{10} k_{ex} K\,[site]}{k'_7} I \tag{38}$$

Eqs. (37) and (38) show that oxidation on the surface of the catalyst via positive holes follows first order kinetic model and k', as a function of UV intensity, is independent of initial 2,4-D concentration (see Eq. (38)).

Similarly, using steady state approximation for the concentration of $OH^{\bullet}_{ads}$ gives:

$$\frac{d[OH^{\bullet}_{ads}]}{dt} = k_7[TiOH][h^{+}]a_s - k_{11}[OH^{\bullet}_{ads}]a_s - k_{ads}[OH^{\bullet}_{ads}][R_{ads}]a_s \cong 0 \tag{39}$$

Therefore,

$$[OH^{\bullet}_{ads}] = \frac{k_7[TiOH][h^{+}]}{k_{11} + k_{ads}[R_{ads}]} \tag{40}$$

Combining Eqs. (35) and (40), leads to:

$$[OH^{\bullet}_{ads}] = \frac{k_7[TiOH]k_{ex}Ia_c}{a_s(k_7[TiOH] + k_{10}[R_{ads}])(k_{11} + k_{ads}[R_{ads}])} \tag{41}$$

As previously explained, $k_7\,[TiOH] \gg k_{10}\,[R_{ads}]$. Thus:

$$[OH^{\bullet}_{ads}] = \frac{k_{ex}Ia_c}{a_s(k_{11} + k_{ads}[R_{ads}])} \tag{42}$$

Combining Eqs. (42) and (30):

$$r_{ads2} = k_{ads}[R_{ads}][OH^{\bullet}_{ads}]a_s = \frac{a_c k_{ex} k_{ads}[R_{ads}]I}{(k_{11} + k_{ads}[R_{ads}])} \tag{43}$$

$$r_{ads2} = \frac{k''\,[R_L]}{1 + \kappa''\,[R_L]} \tag{44}$$

where

$$k'' = \frac{a_c k_{ex} k_{ads} K\,[site]}{k_{11}} I \tag{45}$$

$$\kappa'' = \frac{k_{ads} K\,[site]}{k_{11}} \tag{46}$$

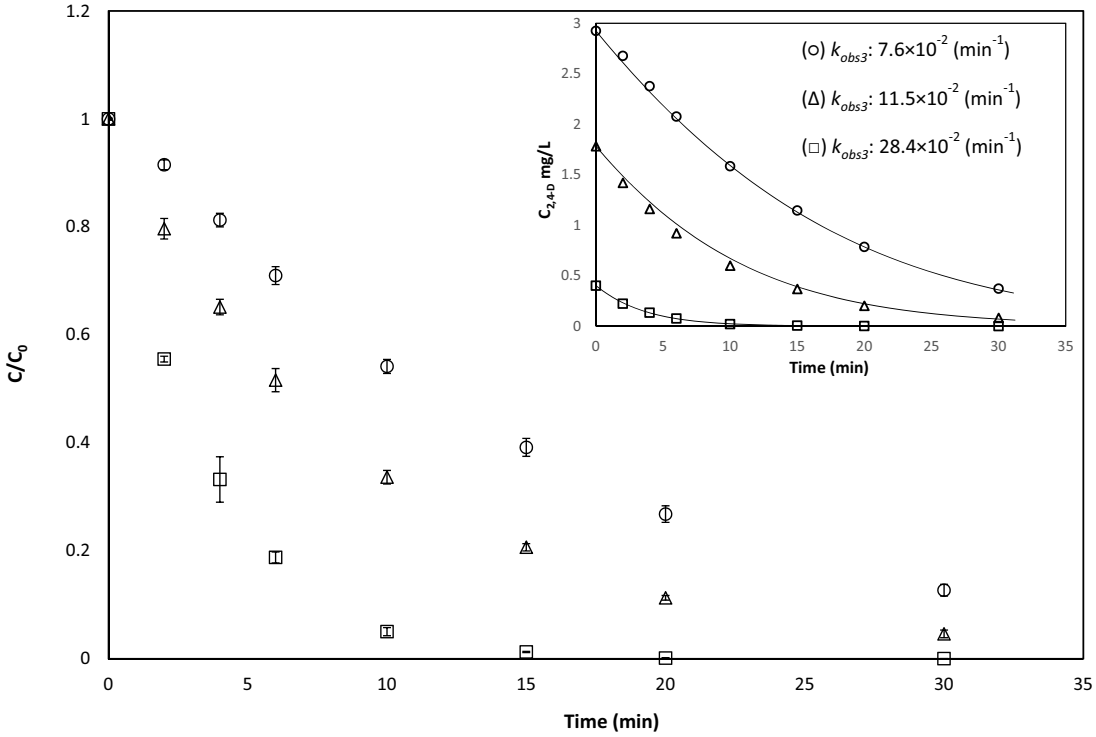

Fig. 6. Photocatalytic oxidation of 2,4-D in a fluidized photocatalytic reactor at pH 3 with different initial concentration of; (□) 1 mgL^{-1}, (Δ) 4 mgL^{-1}, and (○) 7 mgL^{-1}. r_0 represents the initial photocatalytic oxidation rate. Error bars represent the standard errors for the triplicate runs. Full lines represent best-fit curves of the kinetic model developed for photocatalytic oxidation at pH 3.

Eq. (44) shows that oxidation via trapped positive holes follows the L-H model. Furthermore, k'' is a function of intensity and independent of initial 2,4-D concentration.

The concentration of OH°_{aq} at pH 3 can be obtained by combining OH°_{aq} rate balance and Eq. (42):

$$[OH^{\bullet}_{aq}] = \frac{a_c k_{ex} k_{11} I}{a_s (k_{11} + k_{ads}[R_{ads}])(k_{aq}[R_L] + \sum_{i=2}^{n} k_{Ri}[R_{Li}])} \tag{47}$$

By incorporating the above into Eq. (31), the reaction rate of OH°_{aq} with the target contaminant in the solution will be:

$$r_{aq3} = \frac{k''' [R_L]}{1 + \kappa''' [R_L]} \tag{48}$$

$$k''' = \frac{a_c k_{ex}}{a_s [R_{L0}]} I \tag{49}$$

$$\kappa''' = \kappa'' = \frac{k_{ads} K [site]}{k_{11}} \tag{50}$$

Eq. (49) shows that while k''' like k'' and k' is a function of intensity, it depends on the initial concentration of the reactant.

Therefore, the overall rate of 2,4-D degradation at pH 3 will be:

$$r_{pH3} = r_{ads1} + r_{ads2} + r_{aq3} = k' [R_L] + \frac{k_{obs3} [R_L]}{1 + \kappa' [R_L]} \tag{51}$$

$$\text{where} \quad k_{obs3} = k' + k'' = \left(\frac{k_{ads} K [site]}{k_{11}} + \frac{1}{a_s [R_{0L}]} \right) k'_{ex} \tag{52}$$

$$k'_{ex} = a_c k_{ex} I \tag{53}$$

The kinetic models at both acidic and neutral pH were compared with experimental results. Fig. 5 shows that the rate of 2,4-D disappearance at pH 3 is higher than the disappearance rate at pH 7. This difference could be explained based on the different relationships of the rate constants to the intensity at different pH. As is shown in Eqs. (52) and (53), photocatalytic oxidation rate at pH 3 is a function of UV intensity (I), while the rate at pH 7 is related to $(I)^{1/2}$, as shown in Eq. (27).

Table 1
Estimated kinetics parameters for the kinetic model described by Eqs. (51) to (53). 2,4-D photocatalytic oxidation with different initial concentration at pH 3.

Initial concentration (gm^{-3})	$k' \times 10^3$ (min^{-1})	$k'_{ex} \times 10^3$ (g.m^{-1}min^{-1})	$\kappa'' \times 10^3$ (m^{3}g^{-1})
1	10	227	255
4	11	230	222
7	10	201	233

Eq. (51) shows that 2,4-D photocatalytic oxidation kinetic is a combination of L-H and first-order kinetic models at low pH. Oxidation via hydroxyl radicals attack, either on the surface of photocatalyst or in the solution, follows the L-H model, whereas positive hole oxidation is described by first-order kinetic model. Kinetic parameters introduced in Eq. (51) were calculated using least-squares optimization technique (See Table 1) and the results, in agreement with Eq. (52), show that first order kinetic model can interpret the oxidation of 2,4-D at low concentration.

Furthermore, the results (Table 1) show that the kinetic parameters are independent of initial concentration at pH 3. However, k_{obs3} which includes OH°_{aq} and OH°_{ads} rate constants, has an inverse relationship with 2,4-D initial concentration. This is because of 2,4-D intermediates that participate in photocatalytic oxidation via OH°_{aq} in the solution. Fig. 6 shows the photocatalytic oxidation of 2,4-D with different initial concentration at pH 3 alongside the agreement of experimental results with the developed kinetic model. Obviously, results show that the developed model could successfully fit experimental data. Reducing k_{obs3} obtained from the model with increasing 2,4-D initial concentration indicates the effect of 2,4-D initial concentration on k_{obs3} values as estimated in the model.

5. Conclusion

This research focused on the effect of pH on the kinetics of photocatalytic oxidation of 2,4-D, as a model contaminant. The photocatalytic oxidation kinetics changed due to the impact of pH on photocatalyst surface charge and the energies of conductance and valence band. Results showed that the photocatalytic oxidation at $pH > pH_{zpc}$ (pH 7) followed first order kinetic model. At $pH < pH_{zpc}$ (pH 3), on the other hand, the rate of oxidation was a combination of first order and L-H models. Oxidation of 2,4-D intermediates by hydroxyl radicals attack in the solution causes an inverse relationship of observed rate constants with the initial concentration of 2,4-D at low and high pH. Furthermore, according to the kinetic model the dependence of rate constants to UV intensity changed with pH. The rate constant depended on UV intensity at pH 3; however, this parameter showed a square root functionality with respect to intensity at pH 7.

Acknowledgement

The authors would like to acknowledge the Natural Sciences and Engineering Research Council (NSERC) of Canada and RES'EAU-WaterNet Strategic Network (Canada) for financial support. The authors thank the University of British Columbia Bioimaging Facility (Canada) for SEM images.

References

[1] M.R. Hoffmann, S.T. Martin, W. Choi, D.W. Bahnemann, Environmental applications of semiconductor photocatalysis, Chem. Rev. 95 (1995) 69–96.
[2] J. Cunningham, S. Srijaranai, Isotope-effect evidence for hydroxyl radical involvement in alcohol photo-oxidation sensitized by TiO2 in aqueous suspension, J. Photochem. Photobiol. Chem. 43 (1988) 329–335.
[3] R.F. Howe, M. Gratzel, EPR observation of trapped electrons in colloidal titanium dioxide, J. Phys. Chem. 89 (1985) 4495–4499.
[4] H. Liao, T. Reitberger, Generation of free OHaq radicals by black light illumination of degussa (Evonik) P25 TiO2 aqueous suspensions, Catalysts 3 (2013) 418–443.
[5] D.F. Ollis, Kinetics of liquid phase photocatalyzed Reactions: An illuminating approach†, J. Phys. Chem. B. 109 (2005) 2439–2444.
[6] H. Fu, L. Zhang, S. Zhang, Y. Zhu, J. Zhao, Electron spin resonance spin-trapping detection of radical intermediates in N-doped tiO2-Assisted photodegradation of 4-chlorophenol, J. Phys. Chem. B. 110 (2006) 3061–3065.
[7] C.S. Turchi, D.F. Ollis, Photocatalytic degradation of organic water contaminants: mechanisms involving hydroxyl radical attack, J. Catal. 122 (1990) 178–192.
[8] P. Pichat, A brief overview of photocatalytic mechanisms and pathways in water, Water Sci. Technol. 55 (2007) 167.
[9] W.S. Jenks, Photocatalytic reaction pathways –Effects of molecular structure, catalyst, and wavelength, in: P. Pichat (Ed.), Photocatal. Water Purif., Wiley-VCH Verlag GmbH & Co. KGaA, 2013, pp. 25–51.
[10] R. Enríquez, A.G. Agrios, P. Pichat, Probing multiple effects of TiO2 sintering temperature on photocatalytic activity in water by use of a series of organic pollutant molecules, Catal. Today 120 (2007) 196–202.
[11] S. Tunesi, M. Anderson, Influence of chemisorption on the photodecomposition of salicylic acid and related compounds using suspended titania ceramic membranes, J. Phys. Chem. 95 (1991) 3399–3405.
[12] Y. Du, J. Rabani, The measure of TiO2 photocatalytic efficiency and the comparison of different photocatalytic titania, J. Phys. Chem. B. 107 (2003) 11970–11978.
[13] S. Sakthivel, B. Neppolian, M.V. Shankar, B. Arabindoo, M. Palanichamy, V. Murugesan, Solar photocatalytic degradation of azo dye: comparison of photocatalytic efficiency of ZnO and TiO2, Sol. Energy Mater. Sol. Cells 77 (2003) 65–82.
[14] P. Pichat, J.C. D'oliveira, J.F. Maffre, D. Mas, Destruction of 2, 4-dichlorophenoxyethanoic acid (2, 4-D) in water by TiO2-UV, H2O2-UV or direct photolysis, in: D.F. Ollis, H. Al-Ekabi (Eds.), Photocatalytic Purification and Treatment of Water and Air, Elsevier, 1993, pp. 683–688.
[15] O. Legrini, E. Oliveros, A.M. Braun, Photochemical processes for water treatment, Chem. Rev. 93 (1993) 671–698.
[16] Z. Wang, W. Ma, C. Chen, H. Ji, J. Zhao, Probing paramagnetic species in titania-based heterogeneous photocatalysis by electron spin resonance (ESR) spectroscopy—A mini review, Chem. Eng. J. 170 (2011) 353–362.
[17] D.V. Šojić, V.B. Anderluh, D.Z. Orčić, B.F. Abramović, Photodegradation of clopyralid in TiO2 suspensions: identification of intermediates and reaction pathways, J. Hazard. Mater. 168 (2009) 94–101.
[18] U.I. Gaya, Mechanistic Principles of Photocatalytic Reaction, In: Heterog Photocatal. Using Inorg. Semicond. Solids, Springer, Netherlands, 2014, pp. 73–89.
[19] S. Ikeda, N. Sugiyama, S. Murakami, H. Kominami, Y. Kera, H. Noguchi, K. Uosaki, T. Torimoto, B. Ohtani, Quantitative analysis of defective sites in titanium(IV) oxide photocatalyst powders, Phys. Chem. Chem. Phys. 5 (2003) 778–783.
[20] H. de Lasa, B. Serrano, M. Salaices, Kinetic modeling of the photocatalytic reaction network: the parallel-Series approximation, in: Photocatalytic React Eng, Springer, US, 2005, pp. 101–118.
[21] J.E.D. Duran, Development of a CFD-based Model for the Simulation of Immobilized Photocatalytic Reactors for Water Treatment, 2010.
[22] G. Rothenberger, J. Moser, M. Graetzel, N. Serpone, D.K. Sharma, Charge carrier trapping and recombination dynamics in small semiconductor particles, J. Am. Chem. Soc. 107 (1985) 8054–8059.
[23] Y. Nosaka, A.Y. Nosaka, Identification and roles of the active species generated on various photocatalysts, in: P. Pichat (Ed.), Photocatal. Water Purif, Wiley-VCH Verlag GmbH & Co. KGaA, 2013, pp. 1–24.
[24] S.-H. Yoon, S.-E. Oh, J.E. Yang, J.H. Lee, M. Lee, S. Yu, D. Pak, TiO2 photocatalytic oxidation mechanism of As(III), Environ. Sci. Technol. 43 (2009) 864–869.
[25] A. Vega, M. Keshmiri, M. Mohseni, Composite template-free TiO2 photocatalyst: synthesis, characteristics and photocatalytic activity, Appl. Catal. B Environ. 104 (2011) 127–135.
[26] R. Rezaei, M. Mohseni, Impact of natural organic matter on the degradation of 2,4-dichlorophenoxy acetic acid in a fluidized bed photocatalytic reactor, Chem. Eng. J. 310 (Part 2) (2017) 457–463.
[27] A. Avdeef, pKa Determination, pKa Determination, in: Absorpt. Drug Dev. Solubility Permeability Charge State, 2ed ed., John Wiley & Sons, 2012, pp. 31–173.
[28] A. Fujishima, X. Zhang, D.A. Tryk, TiO2 photocatalysis and related surface phenomena, Surf. Sci. Rep. 63 (2008) 515–582.